frontiers | Frontiers in Nanotechnology

TYPE Brief Research Report
PUBLISHED 08 December 2022
DOI 10.3389/fnano.2022.1026635

OPEN ACCESS

EDITED BY
Brandi Cossairt,
University of Washington, United States

REVIEWED BY
Mark Hendricks,
Whitman College, United States
Emil Hernandez-Pagan,
University of Delaware, United States

*CORRESPONDENCE
Alina M. Schimpf,
aschimpf@ucsd.edu

†These authors have contributed equally to this work

SPECIALTY SECTION
This article was submitted to Nanomaterials, a section of the journal Frontiers in Nanotechnology

RECEIVED 24 August 2022
ACCEPTED 21 September 2022
PUBLISHED 08 December 2022

CITATION
Geisenhoff JQ, Yin H, Oget N, Chang H, Chen L and Schimpf AM (2022), Controlled CO labilization of tungsten carbonyl precursors for the low-temperature synthesis of tungsten diselenide nanocrystals. *Front. Nanotechnol.* 4:1026635. doi: 10.3389/fnano.2022.1026635

Controlled CO labilization of tungsten carbonyl precursors for the low-temperature synthesis of tungsten diselenide nanocrystals

Jessica Q. Geisenhoff†, Hang Yin†, Natacha Oget, Haeun Chang, Linfeng Chen and Alina M. Schimpf*

Department of Chemistry and Biochemistry, University of California, San Diego, La Jolla, CA, United States

We report a low-temperature colloidal synthesis of WSe_2 nanocrystals from tungsten hexacarbonyl and diphenyl diselenide in trioctylphosphine oxide (TOPO). We identify TOPO-substituted intermediates, $W(CO)_5$TOPO and *cis*-$W(CO)_4(TOPO)_2$ by infrared spectroscopy. To confirm these assignments, we synthesize aryl analogues of phosphine-oxide-substituted intermediates, $W(CO)_5$TPPO (synthesized previously, TPPO = triphenylphosphine oxide) and *cis*-$W(CO)_4(TPPO)_2$ and *fac*-$W(CO)_3(TPPO)_3$ (new structures reported herein). Ligation of the tungsten carbonyl by either the alkyl or aryl phosphine oxides results in facile labilization of the remaining CO, enabling low-temperature decomposition to nucleate WSe_2 nanocrystals. The reactivity in phosphine oxides is contrasted with syntheses containing phosphine ligands, where substitution results in decreased CO labilization and higher temperatures are required to induce nanocrystal nucleation.

KEYWORDS

tungsten diselenide, transition metal dichalcogenides, nanocrystals, metal carbonyls, precursor reactivity

Introduction

Colloidal synthesis provides an attractive route to solid-state nanomaterials because it can exploit the diverse reaction-parameter-space to obtain kinetic control, enabling access to products that are difficult or impossible to achieve *via* bulk synthetic methods. Understanding and manipulating the precursor chemistry has emerged as a vital tool for advancing nanocrystal syntheses, as precursor conversion governs the nucleation and growth of nanocrystals (Steckel et al., 2006; Liu et al., 2007; Owen et al., 2010; Garcia-Rodriguez and Liu, 2012; Hendricks et al., 2012). Differences in precursor reactivity have been used to tailor nanocrystal size, morphology and phase (Norako and Brutchey, 2010; Hendricks et al., 2015; Campos et al., 2017; Hamachi et al., 2017; Rhodes et al., 2017; Tappan et al., 2018; Geisenhoff et al., 2019; Hernandez-Pagan et al., 2019; Strach et al., 2019; Geisenhoff et al., 2020; Lord et al., 2020; Mantella et al., 2020; Plummer and Hutchison, 2020; Zhou et al., 2021; Bennett et al., 2022). For example, the size and size-

distributions of cadmium, lead, and zinc chalcogenides have been greatly tuned *via* a selection of thioureas and selenoureas to vary the kinetics of the chalcogen supply (Hendricks et al., 2015; Campos et al., 2017; Hamachi et al., 2017; Bennett et al., 2022). In the case of copper nanocrystals, the shape has been selected through manipulation of the ligand-bound copper intermediate to vary the rate of conversion to active monomers (Strach et al., 2019). Specifically, ligation with trioctylphosphine oxide results in rapid conversion and the kinetically favored cubic product, while trioctylphosphine yields the thermodynamically favored spherical nanocrystals. In the synthesis of WSe_2 nanocrystals (Geisenhoff et al., 2019; Zhou et al., 2021), inclusion of trioctylphosphine oxide, oleic acid or oleylamine ligands was shown to vary the precursor reactivity, concomitant with a change in the phase of the final products. We hypothesize that differences in the observed reactivity are due to differences in the decomposition of the tungsten carbonyl precursors, where substitution by ligands at the metal center serves to modulate the energy required for dissociation.

Metal carbonyls, including tungsten hexacarbonyl, molybdenum hexacarbonyl, iron pentacarbonyl, dicobalt octacarbonyl and dimanganese decacarbonyl are widely used in the solution-phase syntheses of metal, metal carbide, metal phosphide or metal chalcogenide nanocrystals, where they are commonly used as a source of metal or as a reducing agent (Hyeon et al., 2001; Puntes et al., 2001; Puntes et al., 2002; Kang et al., 2004; Qian et al., 2004; Lagunas et al., 2006; Lee et al., 2006; Sahoo et al., 2009; Kang and Murray, 2010; Meffre et al., 2012; van Schooneveld et al., 2012; Kang et al., 2013; Jung et al., 2015; Wang et al., 2016; Guo et al., 2017; Liu et al., 2017; Zhao et al., 2017; Huang et al., 2018; Xiao et al., 2018; Geisenhoff et al., 2019; Sokolikova et al., 2019; Zhao et al., 2019; Baddour et al., 2020; Zhou et al., 2021). The use of metal carbonyl precursors generally requires temperatures high enough to force cleavage of the metal–carbonyl bonds (Lewis et al., 1984) and induce nanocrystal nucleation. Metal carbonyls can decompose directly to form metal nanocrystals (Puntes et al., 2001; Puntes et al., 2002; Lagunas et al., 2006; Sahoo et al., 2009; Kang and Murray, 2010; van Schooneveld et al., 2012), or can undergo ligand exchange at the metal site (Angelici, 1968; Werner, 1968; Atwood and Brown, 1976; Darensbourg, 1982; Howell and Burkinshaw, 1983). Such ligand exchange is expected to be important in controlling the subsequent reactivity of the metal carbonyls, but its role in nanocrystal formation has not been explicitly explored. As CO alone has been shown to direct nanocrystal growth and morphology (Kang et al., 2010; Wu et al., 2011), its labilization from metal carbonyls can also be expected to influence nanocrystal formation. Here, we show that the ligands/solvents common in many nanocrystal syntheses play an important role in forming and dictating the reactivity of substituted tungsten carbonyls that are used to form WSe_2 nanocrystals.

We have previously synthesized WSe_2 nanocrystals by hot-injection of diphenyl diselenide (Ph_2Se_2) into tungsten hexacarbonyl ($W(CO)_6$) dissolved in mixtures of trioctylphosphine oxide (TOPO) and oleic acid (OA) at 330°C (Geisenhoff et al., 2019). When using this mixture of ligands, the reactivity is increased with a larger TOPO/OA ratio, leading to more nanocrystal nucleation and smaller nanocrystals that are readily converted to the thermodynamically favored phase (Geisenhoff et al., 2019). Indeed, when OA is excluded, $W(CO)_6$ decomposes at 260°C, prior to injection of Ph_2Se_2 (Geisenhoff et al., 2019). Here, we take advantage of this greater reactivity in TOPO by using a low-temperature injection of Ph_2Se_2 to form WSe_2 nanocrystals at 150°C. We follow the reactivity and conversion of $W(CO)_6$ using IR spectroscopy and show that, prior to Ph_2Se_2 injection, one or two CO ligands are replaced by TOPO ligands, enabling facile CO labilization. In contrast, when just one eq trioctylphosphine (TOP) is included, the TOP-substituted tungsten carbonyl is exclusively formed. This intermediate has decreased ligand dissociation from the tungsten, such that nanocrystals cannot be nucleated below 180°C. The assignment of the phosphine- and phosphine-oxide-substituted intermediates is verified by synthesis of the aryl analogs (TPP and TPPO, respectively; TPP = triphenylphosphine, TPPO = triphenylphosphine oxide), which can be crystallized for structural identification. These studies demonstrate the role that phosphines and phosphine oxides can play in nanocrystal nucleation and growth by dictating the conversion of metal carbonyl precursors.

Results and analysis

WSe_2 nanocrystals were synthesized *via* injection of Ph_2Se_2 into $W(CO)_6$ dissolved in TOPO at 150°C. Briefly, $W(CO)_6$ (20 mg, 0.057 mmol) was heated in TOPO (2.1975 g, 100 TOPO/W) to 150°C and held for 15 min. Beginning at ~ 70°C, the colorless solution began to turn yellow and continued to darken as the temperature increased. This color change was accompanied by bubbling, indicative of some gas evolution. After 15 min at 150°C, Ph_2Se_2 in hexadecane (115 mM, 1 ml, 4 Se/W) was rapidly injected into the W solution. Immediately after injection, the solution changed to brown/black and rapid gas evolution was observed, indicating nucleation of WSe_2 nanocrystals.

Figure 1A0 shows the IR spectrum of an aliquot collected just before the Ph_2Se_2 injection. Here, multiple CO vibrations are observed between 1,950 and 1,850 cm^{-1} (Supplementary Table S1). These vibrations are all shifted to lower wavenumber relative to that of $W(CO)_6$ (1,971 cm^{-1}, Supplementary Figure S1), suggesting that $W(CO)_6$ has undergone substitution by TOPO to form $W(CO)_{6-x}(TOPO)_x$ intermediates. Similar shifts are observed when the CO of $W(CO)_6$ is substituted by one, two or three phosphine oxide ligands (Darensbourg et al., 1986;

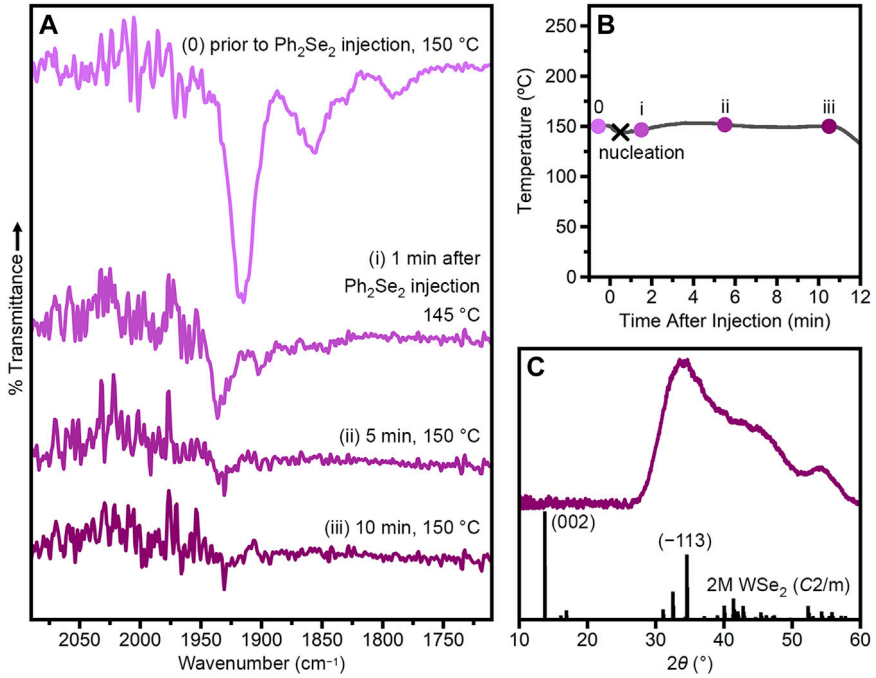

FIGURE 1
Injection of Ph_2Se_2 into $W(CO)_6$ + TOPO (TOPO/Se/W = 100/4/1) at 150°C. **(A)** FTIR spectra of aliquots taken prior to Se injection and approximately 1, 5 and 10 min after Se injection. **(B)** Temperature profile of the reaction with aliquots indicated by circles. The black x indicates the nucleation event, evidenced by a color-change of the reaction solution. **(C)** Powder X-ray diffraction pattern of nanocrystalline product compared to that simulated from single-crystal data for 2M WSe_2 (Fang et al., 2019).

Planinić and Meider, 1989; Cook et al., 2004). Just 1 minute following Ph_2Se_2 injection, the original peaks disappear and are replaced by weak vibrations at 1,937 and 1,903 cm^{-1} (Figure 1Ai), which likely arise from another intermediate formed by oxidative addition of Ph_2Se_2 to the $W(CO)_{6-x}(TOPO)_x$ complexes (Lang et al., 1994a; Lang et al., 1994b; Fortman et al., 2008). Within 10 min following Ph_2Se_2 injection, no CO vibrations are evident in the IR spectrum (Figure 1Aiii), indicating complete conversion of the $W(CO)_{6-x}(TOPO)_x$ intermediates. The heating profile of this synthesis is provided in Figure 1B, with the x indicating nucleation and filled circles indicating when aliquots were taken. After 10 min following Ph_2Se_2 injection, the heating mantle was removed and the resultant nanocrystals were collected, washed and characterized.

Figure 1C shows the powder X-ray diffraction pattern of the resulting nanocrystals. The lack of a (002) reflection suggests very little interlayer stacking, which is confirmed by transmission electron microscopy (Supplementary Figure S2). The most intense reflection is observed at $2\theta \approx 34^{\circ}$, consistent with the (−113) reflection of the metastable 2M phase of WSe_2.(Geisenhoff et al., 2019; Sokolikova et al., 2019; Fang et al., 2019) This phase assignment is corroborated by X-ray photoelectron spectroscopy (Supplementary Figure S3). We have previously shown that increased TOPO/OA leads to more 2H phase when WSe_2 nanocrystals are synthesized at 330°C (Geisenhoff et al., 2019). In this previous work, dominance of the thermodynamically favored phase was due to greater reactivity induced by TOPO, which led to more phase-conversion at high temperatures (Geisenhoff et al., 2019). In contrast, the synthesis presented herein takes advantage of the TOPO-induced reactivity to synthesize WSe_2 nanocrystals at lower temperatures, allowing preservation of the metastable 2M phase.

Since the bulky octyl groups of TOPO prohibit the isolation of single crystals, we used an aryl analog to corroborate the formation of $W(CO)_{6-x}(TOPO)_x$ intermediates. Specifically, we synthesized $W(CO)_{6-x}(TPPO)_x$ (x = 1, 2, 3). $W(CO)_5TPPO$ (Figure 2A) was synthesized from photochemically prepared $W(CO)_5THF$ (THF = tetrahydrofuran) following a previously reported procedure (Darensbourg et al., 1986). To synthesize $W(CO)_4(TPPO)_2$, $W(CO)_6$ and TPPO (10 eq) were combined in toluene and refluxed for ~1 h with stirring. Further addition of toluene resulted in a yellow precipitate, which was redissolved with heat. The resulting solution yielded yellow crystals in ~12 h. Single-crystal X-ray diffraction identified the crystals as *cis*-$W(CO)_4(TPPO)_2$ (Figure 2B, Supplementary Table S2) and powder X-ray

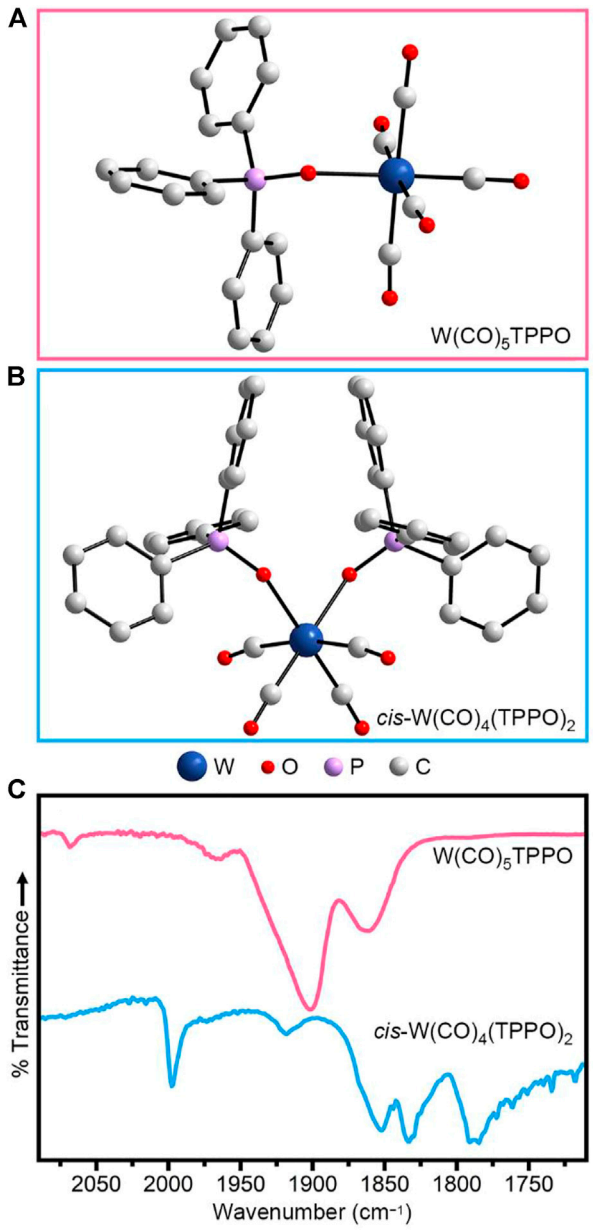

FIGURE 2
Crystal structures of **(A)** $W(CO)_5TPPO$ and **(B)** *cis*-$W(CO)_4(TPPO)_2$. **(C)** FTIR spectra of $W(CO)_5TPPO$ (top) and of *cis*-$W(CO)_4(TPPO)_2$ (bottom) solids.

diffraction confirmed this as the majority product (Supplementary Figure S4). We note, however, that a trace product of *fac*-$W(CO)_3(TPPO)_3$ (Supplementary Table S2, Supplementary Figure S5) was identified by single-crystal X-ray diffraction.

Figure 2C (top, pink) shows the IR spectrum of $W(CO)_5TPPO$. With pseudo-C_{4v} symmetry, this molecule has four IR-active CO vibrations (Supplementary Table S3) (Darensbourg et al., 1986; Cook et al., 2004). Figure 2C (bottom, blue) shows the IR spectrum of *cis*-$W(CO)_4(TPPO)_2$. With pseudo-C_{2v} symmetry, this molecule also has four IR-active CO vibrations (Supplementary Table S4), which are at similar positions to other tungsten carbonyls substituted with two phosphine oxide moieties (Planinić and Meider, 1989). Comparing the IR spectra of these two molecules to that of the pre-injection aliquot (Figure 1A0), we conclude that heating $W(CO)_6$ in TOPO yields a mixture of the mono- and di-substituted species, $W(CO)_5TOPO$ and *cis*-$W(CO)_4(TOPO)_2$, respectively (Supplementary Table S1). The lack of a peak at ~1,970 cm^{-1} indicates little to no remaining $W(CO)_6$, suggesting that $W(CO)_5TOPO$ and *cis*-$W(CO)_4(TOPO)_2$ are the reactive intermediates when Ph_2Se_2 is injected. Phosphine oxides are known to be particularly good at promoting CO labilization in metal carbonyls (Darensbourg et al., 1980; Darensbourg et al., 1981; Darensbourg, 1982), which is likely the reason for increased reactivity when WSe_2 nanocrystals are synthesized in TOPO.

It is worth noting that both increased concentration of $W(CO)_6$ (Supplementary Figure S6) and the addition of a degassing step (Supplementary Figure S7) leads to more substitution by TOPO. When the synthesis is repeated using TPPO instead of TOPO, the reactivity is similar. Specifically, nucleation was observed immediately after the injection of Ph_2Se_2 and WSe_2 nanocrystals are formed within 10 min at 150°C (Supplementary Figure S8). These observations corroborate that the higher reactivity is due to the phosphine oxides.

To contrast the rapid reactivity induced by TOPO, we sought a ligand with stronger binding and decreased CO labilization that would decrease reactivity in the nanocrystal synthesis. TOP is commonly used in nanocrystal syntheses and contains a strong σ-donating, π-accepting phosphine in contrast to the weak, hard oxygen donor of TOPO. Figure 3 shows the characterization of a WSe_2 synthesis performed similarly to that presented in Figure 1, but with just 1 eq TOP added to the reaction mixture. When $W(CO)_6$ is heated at 150°C in the presence of 100 eq TOPO +1 eq TOP for 15 min, IR spectroscopy reveals a new species (Figure 3A0), with vibrations that are distinct from both $W(CO)_6$ and $W(CO)_{6-x}(TOPO)_x$. We assign this species as primarily $W(CO)_5TOP$ with a small amount of $W(CO)_4(TOP)_2$ (Supplementary Table S5, *vide infra*). Importantly, when Ph_2Se_2 is injected into this mixture at 150°C, no color change or gas evolution are observed over the course of 11 min and the CO vibrations remain largely unchanged (Figure 3Ai–iii).

The low reactivity in the presence of TOP is in stark contrast to syntheses without TOP, in which a color-change, gas evolution and loss of CO are observed immediately upon injection (Figures 1A, B). To induce nanocrystal nucleation, the reaction was heated to 250°C over ~10 min (Figure 3B). As the temperature was increased, the solution began to turn brown, indicating nucleation of WSe_2. This color-change was accompanied by

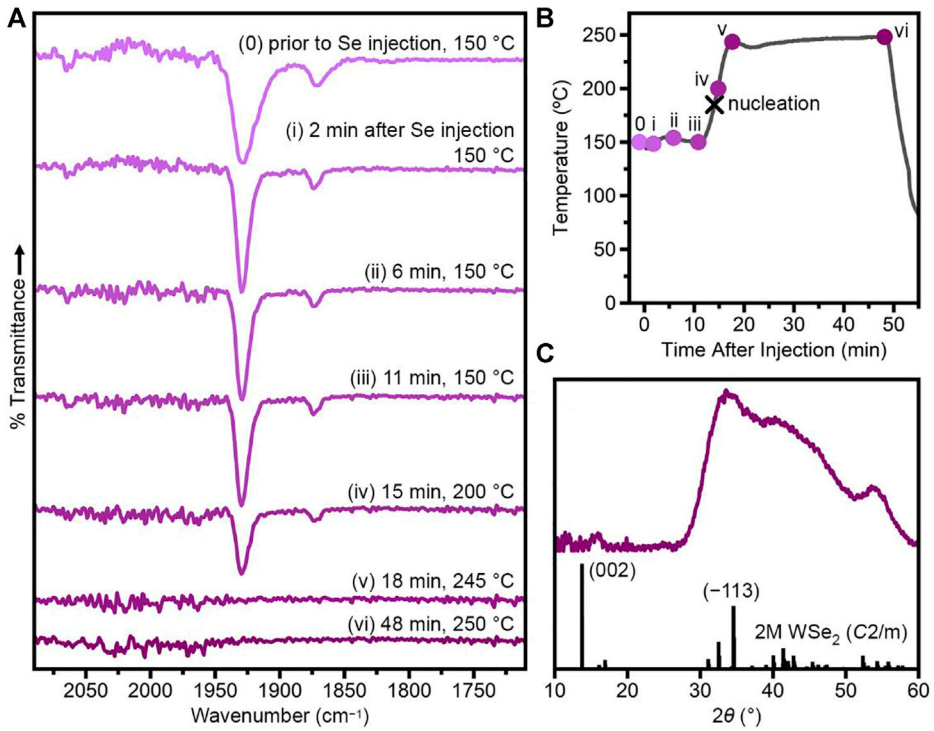

FIGURE 3
Injection of Ph_2Se_2 into $W(CO)_6$ + TOPO + TOP (TOPO/TOP/Se/W = 100/1/4/1) at 150°C. **(A)** FTIR spectra of aliquots taken prior to Se injection and approximately 2, 6, 11, 15, 18 and 48 min after Se injection. **(B)** Temperature profile of the reaction with aliquots indicated by circles. The black x indicates the nucleation event, evidenced by a color-change of the reaction solution. **(C)** Powder X-ray diffraction pattern of nanocrystalline product compared to that simulated from single-crystal data for 2M WSe_2 (Fang et al., 2019).

gas evolution, indicating liberation of CO. When the temperature reached 250°C, the solution was very dark brown and gas evolution had slowed. Aliquots were collected shortly after nucleation (Figures 3A, Biv), once the temperature reached 250°C (Figures 3A,Bv) and after 30 min at 250°C (Figures 3A, Bvi). The intensity of the $W(CO)_5$TOP CO vibration at 1,930 cm^{-1} decreased following WSe_2 nucleation, and disappeared completely by the time the temperature reached 250°C. Powder X-ray diffraction (Figure 3C) on the final nanocrystalline product reveals 2M WSe_2.

To confirm the assignment of $W(CO)_5$TOP, we synthesized the aryl analog, $W(CO)_5$TPP (Figure 4A) using previously reported methods (Aroney et al., 1994). Figure 4bi shows the IR spectrum of crystals of $W(CO)_5$TPP dissolved in THF. With pseaudo-C_{4v} symmetry, this molecule is expected to have four IR-active CO vibrations, but in this case the A_1 (2) and E modes are unresolvable (Supplementary Table S6) (Cotton and Kraihanzel, 1962; Angelici and Malone, 1967). Importantly, when $W(CO)_5$TPP is heated in 100 eq TOPO at 150°C for 15 min (Figure 4Bii), the IR spectrum is comparable to that of the TOP-containing syntheses prior to injection of Ph_2Se_2 (Figure 3A0), and can be assigned primarily to $W(CO)_5$TPP with a small amount of $W(CO)_4(TPP)_2$ (Supplementary Table S7). All peaks are shifted to slightly higher wavenumber for TPP-substituted species relative to the TOP-substituted species due to the electron-withdrawing nature of the phenyl substituents (Cotton et al., 1981; Honeychuck and Hersh, 1987).

When Ph_2Se_2 is injected into $W(CO)_5$TPP +100 eq TOPO at 150°C, the reactivity is similar to that of the TOP-containing synthesis. Specifically, no color-change or gas evolution were observed over 10 min and the $W(CO)_5$TPP CO vibration at 1,937 cm^{-1} persisted, although with some decrease in intensity. We note that, in this synthesis, the CO vibration assigned to $W(CO)_4(TPP)_2$ disappears upon injection of Ph_2Se_2. We hypothesize that this is due to conversion of $W(CO)_4(TPP)_2$ to $W(CO)_5$TPP. This conversion results in formation of a small amount of TPP=Se and Ph_2Se (Supplementary Equation S1), neither of which can react directly with $W(CO)_5$TPP to nucleate nanocrystals at 150°C. When the reaction is further heated, a color change is observed, indicating nucleation of WSe_2 (Supplementary Figure S9B). The reactivity of $W(CO)_5$TPP is greater than that of the TOP-containing synthesis, likely due to the electron-withdrawing nature of the phenyl substituents. Both phosphine-substituted species, however, show delayed reactivity compared to synthesis in TOPO alone. This observation confirms that carbonyl substitution with phosphines or

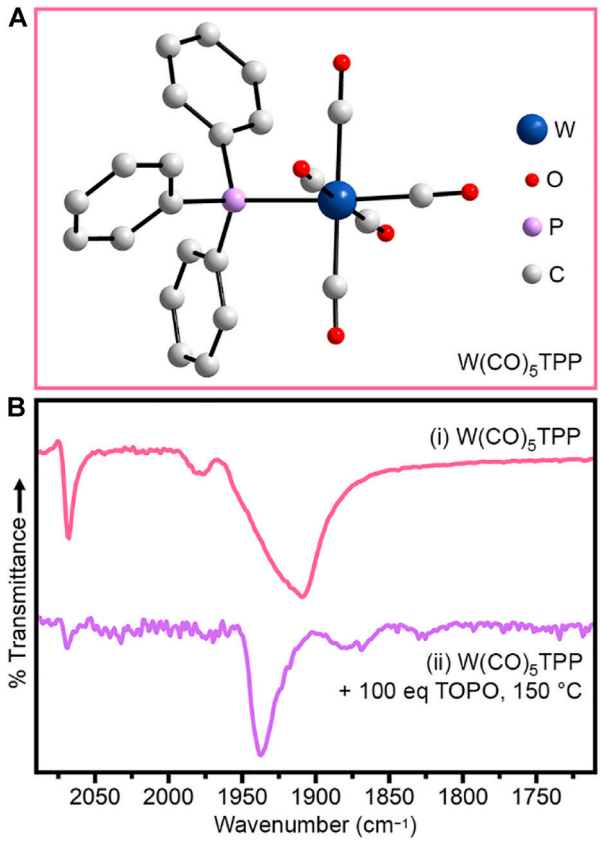

FIGURE 4
(A) Crystal structure of $W(CO)_5TPP$. **(B)** IR spectra of **(i)** $W(CO)_5TPP$ dried solid and of (ii) that solid heated in 100 eq TOPO to 150°C for 15 min (bottom). All spectra were collected at room-temperature.

phosphine oxides can be used to delay or induce nanocrystal nucleation, respectively.

Discussion

The decrease in reactivity observed with the phosphine substitution compared to phosphine-oxide substitution is likely two-fold. First, the phosphine is a stronger σ-donating and π-accepting ligand, making it less labile than the phosphine oxide ligand (Wovkulich and Atwood, 1980). Second, phosphine- and phosphite-substitution in metal carbonyls have been shown to decrease CO labilization (Angelici and Graham, 1965; Angelici and Graham, 1967; Angelici, 1968; Werner, 1968; Parker and Wojcicki, 1974; Atwood and Brown, 1976; Darensbourg et al., 1981; Cotton et al., 1982; Howell and Burkinshaw, 1983). In contrast, substitution with hard donor ligands (Angelici and Graham, 1967; Angelici, 1968; Werner, 1968; Brown and Dobson, 1972; Parker and Wojcicki, 1974; Howell and Burkinshaw, 1983), including phosphine oxides (Darensbourg et al., 1980; Darensbourg et al., 1981; Darensbourg, 1982), has been shown to increase CO labilization in metal carbonyls. This has been explained due to σ- and π-bonding effects between the donor and central metal atom, as well as a result of direct donation from the filled σ_z^b orbital of the donor to the π* orbitals of the carbonyls cis to the donor (Fenske and Dekock, 1970; Parker and Wojcicki, 1974; Howell and Burkinshaw, 1983). The low lability of both the phosphine and carbonyl ligands inhibits coordination by the Se precursor, thus requiring higher temperatures to force cleavage of the W–C and/or W–P bonds to initiate WSe_2 nucleation. We note that the substituents of the phosphine ligand also play a significant role in modifying the reactivity of the substituted metal carbonyls. With direct coordination to the donor, electron-withdrawing groups (e.g. phenyl substituents) decrease the P–W bond strength to allow for ligand dissociation at lower temperatures. This effect is not present in the phosphine oxides, as the substituents are not well-coupled to the donor.

In our hands, $W(CO)_6$ does not dissolve well in noncoordinating solvents used for nanocrystal synthesis, such as hexadecane. Thus, the influence on reactivity of a coordinating solvent will likely be an important consideration. The reactivity trend observed with phosphine oxides vs. phosphines can possibly be extended to other common nanocrystal ligands/solvents based on the known reactivity with metal carbonyls. For example, oleylamine would also be expected to be CO-labilizing due to the hard N donor (Angelici and Graham, 1967; Angelici, 1968; Werner, 1968; Brown and Dobson, 1972; Parker and Wojcicki, 1974; Howell and Burkinshaw, 1983), and could facilitate metal carbonyl decomposition (Zhao et al., 2017). Variation of the substituents on the N donor could be used to further tune the reactivity. We note that we have not discussed the role of steric interactions, which could be used to further modify the metal carbonyl stability.

Summary and conclusion

We present a low-temperature synthesis of WSe_2 nanocrystals by taking advantage of the modified reactivity of substituted tungsten carbonyls. When nanocrystals are synthesized in TOPO, $W(CO)_5TOPO$ and *cis*-$W(CO)_4(TOPO)_2$ are identified as the reactive tungsten intermediates. This substitution with TOPO enables facile CO labilization, allowing for the ligand dissociation required to initiate reactivity of the tungsten carbonyls with the Se precursor at 150°C. In contrast, when just 1 eq TOP is included, nanocrystals cannot be nucleated below 180°C due to the non-labilizing nature of the phosphine. The reactivity of phosphine-containing syntheses can be further tuned *via* choice of phosphine substituent, where electron-withdrawing groups lead to increased reactivity. These results demonstrate the influence of common nanocrystal ligands on metal carbonyl

reactivity and offer insight for fine-tuning the reactivity to manipulate nanocrystal nucleation and growth.

Data availability statement

The raw data supporting the conclusions of this article will be made available by the authors, without undue reservation.

Author contributions

All authors listed have made a substantial, direct, and intellectual contribution to the work and approved it for publication.

Funding

This research was supported by the U. S. National Science Foundation (CHE-2003675 to AS). XPS data were collected at the UC Irvine Materials Research Institute using instrumentation funded in part by the National Science Foundation Major Research Instrumentation Program (CHE-1338173).

Conflict of interest

The authors declare that the research was conducted in the absence of any commercial or financial relationships that could be construed as a potential conflict of interest.

Publisher's note

All claims expressed in this article are solely those of the authors and do not necessarily represent those of their affiliated organizations, or those of the publisher, the editors and the reviewers. Any product that may be evaluated in this article, or claim that may be made by its manufacturer, is not guaranteed or endorsed by the publisher.

Supplementary material

The Supplementary Material for this article can be found online at: https://www.frontiersin.org/articles/10.3389/fnano.2022.1026635/full#supplementary-material

References

Angelici, R. J., and Graham, J. R. (1965). Kinetic studies of group VI metal carbonyl complexes. I. Substitution reactions of dipyridyl complexes of chromium Hexacarbonyl[1]. *J. Am. Chem. Soc.* 87, 5586–5590. doi:10.1021/ja00952a013

Angelici, R. J., and Graham, J. R. (1967). Kinetic studies of Group VI metal carbonyl complexes. IV. Substitution reactions of o-phenanthroline complexes of chromium hexacarbonyl. *Inorg. Chem.* 6, 988–992. doi:10.1021/ic50051a029

Angelici, R. J. (1968). Kinetics and mechanisms of substitution reactions of metal carbonyl complexes. *Organomet. Chem. Rev.* 3, 173.

Angelici, R. J., and Malone, M. D. (1967). Infrared studies of amine pyridine and phosphine derivatives of tungsten hexacarbonyl. *Inorg. Chem.* 6, 1731–1736. doi:10.1021/ic50055a026

Aroney, M. J., Buys, I. E., Davies, M. S., and Hambley, T. W. (1994). Crystal-structures of $[W(CO)_5(PPh_3)]$, $[M(CO)_5(AsPh_3)]$ and $[M(CO)_5(SbPh_3)]$ (M = Mo or W): A comparative study of structure and bonding in $[M(CO)_5(EPh_3)]$ complexes (E = P, as or Sb; M = Cr, Mo or W). *J. Chem. Soc. Dalton Trans.* 1994, 2827. doi:10.1039/dt9940002827

Atwood, J. D., and Brown, T. L. (1976). Cis labilization of ligand dissociation. 3. Survey of group 6 and 7 six-coordinate carbonyl compounds. The site preference model for ligand labilization effects. *J. Am. Chem. Soc.* 98, 3160–3166. doi:10.1021/ja00427a017

Baddour, F. G., Roberts, E. J., To, A. T., Wang, L., Habas, S. E., Ruddy, D. A., et al. (2020). An exceptionally mild and scalable solution-phase synthesis of molybdenum carbide nanoparticles for thermocatalytic CO2 hydrogenation. *J. Am. Chem. Soc.* 142, 1010–1019. doi:10.1021/jacs.9b11238

Bennett, E., Greenberg, M. W., Jordan, A. J., Hamachi, L. S., Banerjee, S., Billinge, S. J. L., et al. (2022). Size dependent optical properties and structure of ZnS nanocrystals prepared from a library of thioureas. *Chem. Mat.* 34, 706–717. doi:10.1021/acs.chemmater.1c03432

Brown, R. A., and Dobson, G. R. (1972). Octahedral metal carbonyls. XXI. Carbonyl and metal–carbon stretching spectra of monosubstituted group vib metal carbonyls. *Inorganica Chim. Acta* 6, 65–71. doi:10.1016/s0020-1693(00)91760-2

Campos, M. P., Hendricks, M. P., Beecher, A. N., Walravens, W., Swain, R. A., Cleveland, G. T., et al. (2017). A library of selenourea precursors to PbSe nanocrystals with size distributions near the homogeneous limit. *J. Am. Chem. Soc.* 139, 2296–2305. doi:10.1021/jacs.6b11021

Cook, J. B., Nicholson, B. K., and Smith, D. W. (2004). A structural, spectroscopic and theoretical study of the triphenylphosphine chalcogenide complexes of tungsten carbonyl, $[W(XPPh_3)(CO)_5]$, X = O, S, Se. *J. Organomet. Chem.* 689, 860–869. doi:10.1016/j.jorganchem.2003.12.016

Cotton, F. A., Darensbourg, D. J., and Ilsley, W. H. (1981). Acidity of tris(2-cyanoethyl)phosphine. X-Ray structural studies of $M(CO)_5P(CH_2CH_2CN)_3$ (M = Cr, Mo) and $Mo(CO)_5P(C_6H_5)_3$. *Inorg. Chem.* 20, 578–583. doi:10.1021/ic50216a051π

Cotton, F. A., Darensbourg, D. J., Kolthammer, B. W. S., and Kudaroski, R. (1982). Solid-state and solution structures of [PNP] $[W(CO)_5O_2CCH_3]$ and [PNP] $[W(CO)_4(PEt_3)O_2CCH_3]$ and the CO-labilizing ability of the acetato ligand in these anionic derivatives. *Inorg. Chem.* 21, 1656–1662. doi:10.1021/ic00134a076

Cotton, F. A., and Kraihanzel, C. S. (1962). Vibrational spectra and bonding in metal carbonyls. I. Infrared spectra of phosphine-substituted group VI carbonyls in the CO stretching region. *J. Am. Chem. Soc.* 84, 4432–4438. doi:10.1021/ja00882a012

Darensbourg, D. J., Darensbourg, M. Y., and Walker, N. (1981). Studies using $(n\text{-}Bu)_3P{=}O$ as a carbon monoxide labilizing ligand in the synthesis of metal carbonyl complexes highly enriched in ^{13}CO. *Inorg. Chem.* 20, 1918–1921. doi:10.1021/ic50220a059

Darensbourg, D. J. (1982). Mechanistic pathways for ligand substitution processes in metal carbonyls. *Adv. Organomet. Chem.* 21, 113.

Darensbourg, D. J., Pala, M., Simmons, D., and Rheingold, A. L. (1986). Chemical and structural characterization of $W(CO)_5OPPh_2NPPh_3$. A novel complex containing a phosphine oxide ligand derived from the bis(triphenylphosphine) nitrogen(1+) cation. *Inorg. Chem.* 25, 3537–3541. doi:10.1021/ic00239a047

Darensbourg, D. J., Walker, N., and Darensbourg, M. Y. (1980). Synthesis of metal carbonyl complexes highly enriched in carbon-13: Utilization of the CO-labilizing ability of $(n\text{-}Bu)_3P{=}O$. *J. Am. Chem. Soc.* 102, 1213–1214. doi:10.1021/ja00523a075

Fang, Y. Q., Dong, Q., Pan, J., Liu, H. Y., Liu, P., Sun, Y. Y., et al. (2019). Observation of superconductivity in pressurized 2M WSe_2 crystals. *J. Mat. Chem. C* 7, 8551–8555. doi:10.1039/c9tc02417d

Fenske, R. F., and Dekock, R. L. (1970). Electronic structure and bonding in manganese pentacarbonyl halides and hydride. *Inorg. Chem.* 9, 1053–1060. doi:10.1021/ic50087a010

Fortman, G. C., Kegl, T., and Hoff, C. D. (2008). Kinetic, thermodynamic, and mechanistic aspects of oxidative addition reactions of RE-ER (E = S, Se, Te) and transition metal complexes. *Curr. Org. Chem.* 12, 1279–1297. doi:10.2174/138527208785909574

Garcia-Rodriguez, R., and Liu, H. T. (2012). Mechanistic study of the synthesis of CdSe nanocrystals: Release of selenium. *J. Am. Chem. Soc.* 134, 1400–1403. doi:10.1021/ja209246z

Geisenhoff, J. Q., Tamura, A. K., and Schimpf, A. M. (2020). Manipulation of precursor reactivity for the facile synthesis of heterostructured and hollow metal selenide nanocrystals. *Chem. Mat.* 32, 2304–2312. doi:10.1021/acs.chemmater.9b04305

Geisenhoff, J. Q., Tamura, A. K., and Schimpf, A. M. (2019). Using ligands to control reactivity, size and phase in the colloidal synthesis of WSe_2 nanocrystals. *Chem. Commun.* 55, 8856–8859. doi:10.1039/c9cc03326b

Guo, W. B., Chen, Y. Z., Wang, L. S., Xu, J., Zeng, D. Q., and Peng, D. L. (2017). Colloidal synthesis of $MoSe_2$ nanonetworks and nanoflowers with efficient electrocatalytic hydrogen-evolution activity. *Electrochim. Acta* 231, 69–76. doi:10.1016/j.electacta.2017.02.048

Hamachi, L. S., Plante, I. J. L., Coryell, A. C., De Roo, J., and Owen, J. S. (2017). Kinetic control over CdS nanocrystal nucleation using a library of thiocarbonates, thiocarbamates, and thioureas. *Chem. Mat.* 29, 8711–8719. doi:10.1021/acs.chemmater.7b02861

Hendricks, M. P., Campos, M. P., Cleveland, G. T., Jen-La Plante, I., and Owen, J. S. (2015). A tunable library of substituted thiourea precursors to metal sulfide nanocrystals. *Science* 348, 1226–1230. doi:10.1126/science.aaa2951

Hendricks, M. P., Cossairt, B. M., and Owen, J. S. (2012). The importance of nanocrystal precursor conversion kinetics: Mechanism of the reaction between cadmium carboxylate and cadmium bis(diphenyldithiophosphinate). *Acs Nano* 6, 10054–10062. doi:10.1021/nn303769h

Hernandez-Pagan, E. A., Robinson, E. H., La Croix, A. D., and Macdonald, J. E. (2019). Direct synthesis of novel $Cu_{2-x}Se$ wurtzite phase. *Chem. Mat.* 31, 4619–4624. doi:10.1021/acs.chemmater.9b02019

Honeychuck, R. V., and Hersh, W. H. (1987). Observation of a novel ^{31}P NMR cis-influence series: Implications for the relative basicity of PPh3 and PMe_3 in tungsten carbonyl complexes. *Inorg. Chem.* 26, 1826–1828. doi:10.1021/ic00258a042

Howell, J. A. S., and Burkinshaw, P. M. (1983). Ligand substitution reactions at low-valent four-five-and six-coordinate transition metal centers. *Chem. Rev.* 83, 557–599. doi:10.1021/cr00057a005

Huang, L., Zhang, X. P., Wang, Q. Q., Han, Y. J., Fang, Y. X., and Dong, S. J. (2018). Shape-control of Pt-Ru nanocrystals: Tuning surface structure for enhanced electrocatalytic methanol oxidation. *J. Am. Chem. Soc.* 140, 1142–1147. doi:10.1021/jacs.7b12353

Hyeon, T., Lee, S. S., Park, J., Chung, Y., and Bin Na, H. (2001). Synthesis of highly crystalline and monodisperse maghemite nanocrystallites without a size-selection process. *J. Am. Chem. Soc.* 123, 12798–12801. doi:10.1021/ja016812s

Jung, W., Lee, S., Yoo, D., Jeong, S., Miro, P., Kuc, A., et al. (2015). Colloidal synthesis of single-layer MSe_2 (M = Mo, W) nanosheets via anisotropic solution-phase growth approach. *J. Am. Chem. Soc.* 137, 7266–7269. doi:10.1021/jacs.5b02772

Kang, E., Park, J., Hwang, Y., Kang, M., Park, J. G., and Hyeon, T. (2004). Direct synthesis of highly crystalline and monodisperse manganese ferrite nanocrystals. *J. Phys. Chem. B* 108, 13932–13935. doi:10.1021/jp049041y

Kang, Y. J., and Murray, C. B. (2010). Synthesis and electrocatalytic properties of cubic Mn-Pt nanocrystals (nanocubes). *J. Am. Chem. Soc.* 132, 7568–7569. doi:10.1021/ja100705j

Kang, Y. J., Ye, X. C., and Murray, C. B. (2010). Size- and shape-selective synthesis of metal nanocrystals and nanowires using CO as a reducing agent. *Angew. Chem. Int. Ed.* 49, 6156–6159. doi:10.1002/anie.201003383

Kang, Y., Pyo, J. B., Ye, X., Diaz, R. E., Gordon, T. R., Stach, E. A., et al. (2013). Shape-controlled synthesis of Pt nanocrystals: The role of metal carbonyls. *ACS Nano* 7, 645–653. doi:10.1021/nn3048439

Lagunas, A., Jimeno, C., Font, D., Sola, L., and Pericas, M. A. (2006). Mechanistic studies on the conversion of dicobalt octacarbonyl into colloidal cobalt nanoparticles. *Langmuir* 22, 3823–3829. doi:10.1021/la053016h

Lang, R. F., Ju, T. D., Kiss, G., Hoff, C. D., Bryan, J. C., and Kubas, G. J. (1994). Oxidative addition of disulfides to the complex $W(CO)_3(phen)(EtCN)$. Synthesis, structure, and reactivity of $W(CO)_2(phen)(SR)_2$ (R = Ph, me, CH_2Ph, ^tBu; phen = 1, 10-phenanthroline) coordinatively unsaturated complexes of tungsten(II) that reversibly bind CO and other ligands. *Inorg. Chem.* 33, 3899–3907. doi:10.1021/ic00096a013

Lang, R. F., Ju, T. D., Kiss, G., Hoff, C. D., Bryan, J. C., and Kubas, G. J. (1994). Oxidative addition of thiols, disulfides, iodine, and hydrogen iodide to $W(CO)_3(P^iPr_3)_2$. Preparation of stable 17-electron tungsten thiolate radicals from complexes with weak W-H bonds. *J. Am. Chem. Soc.* 116, 7917–7918. doi:10.1021/ja00096a067

Lee, D. C., Ghezelbash, A., Stowell, C. A., and Korgel, B. A. (2006). Synthesis and magnetic properties of colloidal MnPt3 nanocrystals. *J. Phys. Chem. B* 110, 20906–20911. doi:10.1021/jp064050n

Lewis, K. E., Golden, D. M., and Smith, G. P. (1984). Organometallic bond dissociation energies: Laser pyrolysis of $Fe(CO)_5$, $Cr(CO)_6$, $Mo(CO)_6$, and $W(CO)_6$. *J. Am. Chem. Soc.* 106, 3905–3912. doi:10.1021/ja00326a004

Liu, H. T., Owen, J. S., and Alivisatos, A. P. (2007). Mechanistic study of precursor evolution in colloidal group II–VI semiconductor nanocrystal synthesis. *J. Am. Chem. Soc.* 129, 305–312. doi:10.1021/ja0656696

Liu, M., Wang, Z. J., Liu, J. X., Wei, G. J., Du, J., Li, Y. P., et al. (2017). Synthesis of few-layer 1t'-$MoTe_2$ ultrathin nanosheets for high-performance pseudocapacitors. *J. Mat. Chem. A* 5, 1035–1042. doi:10.1039/c6ta08206h

Lord, R. W., Fanghanel, J., Holder, C. F., Dabo, I., and Schaak, R. E. (2020). Colloidal nanoparticles of a metastable copper selenide phase with near-infrared plasmon resonance. *Chem. Mat.* 32, 10227–10234. doi:10.1021/acs.chemmater.0c04058

Mantella, V., Varandili, S. B., Pankhurst, J. R., and Buonsanti, R. (2020). Colloidal synthesis of Cu-M-S (M = V, Cr, Mn) nanocrystals by tuning the copper precursor reactivity. *Chem. Mat.* 32, 9780–9786. doi:10.1021/acs.chemmater.0c03788

Meffre, A., Mehdaoui, B., Kelsen, V., Fazzini, P. F., Carrey, J., Lachaize, S., et al. (2012). A simple chemical route toward monodisperse iron carbide nanoparticles displaying tunable magnetic and unprecedented hyperthermia properties. *Nano Lett.* 12, 4722–4728. doi:10.1021/nl302160d

Norako, M. E., and Brutchey, R. L. (2010). Synthesis of metastable wurtzite $CuInSe_2$ nanocrystals. *Chem. Mat.* 22, 1613–1615. doi:10.1021/cm100341r

Owen, J. S., Chan, E. M., Liu, H. T., and Alivisatos, A. P. (2010). Precursor conversion kinetics and the nucleation of cadmium selenide nanocrystals. *J. Am. Chem. Soc.* 132, 18206–18213. doi:10.1021/ja106777j

Parker, P. J., and Wojcicki, A. (1974). Kinetic studies of carbonyl substitution in quinolinolatotetracarbonylmanganese(I) and its tricarbonyl derivatives. *Inorganica Chim. Acta* 11, 17–23. doi:10.1016/s0020-1693(00)93686-7

Planinić, P., and Meider, H. (1989). Synthesis and characterization of molybdenum(0) and tungsten(0) carbonyl derivatives of methylenebis [diphenylphosphine oxide] and bis[diphenylphosphinyl)methyl]phenylphosphine oxide. *Polyhedron* 8, 627–632. doi:10.1016/s0277-5387(00)83824-3

Plummer, L. K., and Hutchison, J. E. (2020). Understanding the effects of iron precursor ligation and oxidation state leads to improved synthetic control for spinel iron oxide nanocrystals. *Inorg. Chem.* 59, 15074–15087. doi:10.1021/acs.inorgchem.0c02040

Puntes, V. F., Krishnan, K. M., and Alivisatos, A. P. (2001). Colloidal nanocrystal shape and size control: The case of cobalt. *Science* 291, 2115–2117. doi:10.1126/science.1058495

Puntes, V. F., Zanchet, D., Erdonmez, C. K., and Alivisatos, A. P. (2002). Synthesis of hcp-Co nanodisks. *J. Am. Chem. Soc.* 124, 12874–12880. doi:10.1021/ja027262g

Qian, C., Kim, F., Ma, L., Tsui, F., Yang, P., and Liu, J. (2004). Solution-phase synthesis of single-crystalline iron phosphide nanorods/nanowires. *J. Am. Chem. Soc.* 126, 1195–1198. doi:10.1021/ja038401c

Rhodes, J. M., Jones, C. A., Thal, L. B., and Macdonald, J. E. (2017). Phase-controlled colloidal syntheses of iron sulfide nanocrystals via sulfur precursor reactivity and direct pyrite precipitation. *Chem. Mat.* 29, 8521–8530. doi:10.1021/acs.chemmater.7b03550

Sahoo, P. K., Kamal, S. S. K., Premkumar, M., Kumar, T. J., Sreedhar, B., Singh, A. K., et al. (2009). Synthesis of tungsten nanoparticles by solvothermal decomposition of tungsten hexacarbonyl. *Int. J. Refract. Met. Hard Mat.* 27, 784–791. doi:10.1016/j.ijrmhm.2009.01.005

Sokolikova, M. S., Sherrell, P. C., Palczynski, P., Bemmer, V. L., and Mattevi, C. (2019). Direct solution-phase synthesis of 1T′ WSe_2 nanosheets. *Nat. Commun.* 10, 712. doi:10.1038/s41467-019-08594-3

Steckel, J. S., Yen, B. K. H., Oertel, D. C., and Bawendi, M. G. (2006). On the mechanism of lead chalcogenide nanocrystal formation. *J. Am. Chem. Soc.* 128, 13032–13033. doi:10.1021/ja062626g

Strach, M., Mantella, V., Pankhurst, J. R., Iyengar, P., Loiudice, A., Das, S., et al. (2019). Insights into reaction intermediates to predict synthetic pathways for shape-controlled metal nanocrystals. *J. Am. Chem. Soc.* 141, 16312–16322. doi:10.1021/jacs.9b06267

Tappan, B. A., Barim, G., Kwok, J. C., and Brutchey, R. L. (2018). Utilizing diselenide precursors toward rationally controlled synthesis of metastable

CuInSe2 nanocrystals. *Chem. Mat.* 30, 5704–5713. doi:10.1021/acs.chemmater.8b02205

van Schooneveld, M. M., Campos-Cuerva, C., Pet, J., Meeldijk, J. D., van Rijssel, J., Meijerink, A., et al. (2012). Composition tunable cobalt-nickel and cobalt-iron alloy nanoparticles below 10 NM synthesized using acetonated cobalt carbonyl. *J. Nanopart. Res.* 14, 991. doi:10.1007/s11051-012-0991-5

Wang, Z. C., Chen, Y. Z., Zeng, D. Q., Zhang, Q. F., and Peng, D. L. (2016). Solution synthesis of triangular and hexagonal nickel nanosheets with the aid of tungsten hexacarbonyl. *CrystEngComm* 18, 1295–1301. doi:10.1039/c5ce02187a

Werner, H. (1968). Kinetic studies on substitution reactions of carbonylmetal complexes. *Angew. Chem. Int. Ed. Engl.* 7, 930–941. doi:10.1002/anie.196809301

Wovkulich, M. J., and Atwood, J. D. (1980). Ligand dissociation from mono-substituted derivatives of hexacarbonylchromium (Cr(CO)5L, L = $P(C_6H_5)_3$, $P(C_4H_9)_3$, $P(OCH_3)_3$, $P(OC_6H_5)_3$, and $as(C_6H_5)_3$). *J. Organomet. Chem.* 184, 77–89. doi:10.1016/s0022-328x(00)94365-1

Wu, B. H., Zheng, N. F., and Fu, G. (2011). Small molecules control the formation of Pt nanocrystals: A key role of carbon monoxide in the synthesis of Pt nanocubes. *Chem. Commun.* 47, 1039–1041. doi:10.1039/c0cc03671d

Xiao, L., Zhou, T., Chen, Y. Z., Wang, Z. C., Zheng, H. F., Xu, W. J., et al. (2018). Tungsten hexacarbonyl-induced growth of nickel nanorods and nanocubes. *Mat. Lett.* 229, 340–343. doi:10.1016/j.matlet.2018.07.056

Zhao, X. X., Di, Q., Li, M. R., Yang, Q., Zhang, Z. Y., Guo, X. Y., et al. (2019). Generalized synthesis of uniform metal nanoparticles assisted with tungsten hexacarbonyl. *Chem. Mat.* 31, 4325–4329. doi:10.1021/acs.chemmater.9b00219

Zhao, X. X., Di, Q., Wu, X. T., Liu, Y. B., Yu, Y. K., Wei, G. J., et al. (2017). Mild synthesis of monodisperse tin nanocrystals and tin chalcogenide hollow nanostructures. *Chem. Commun.* 53, 11001–11004. doi:10.1039/c7cc06729a

Zhou, P. S., Schiettecatte, P., Vandichel, M., Rousaki, A., Vandenabeele, P., Hens, Z., et al. (2021). Synthesis of colloidal WSe_2 nanocrystals: Polymorphism control by precursor-ligand chemistry. *Cryst. Growth Des.* 21, 1451–1460. doi:10.1021/acs.cgd.0c01036